Journal of Computational and Applied Mathematics 343 (2018) 124–138

Contents lists available at ScienceDirect

Journal of Computational and Applied Mathematics

journal homepage: www.elsevier.com/locate/cam

Isogeometric boundary element method for calculating effective property of steady state thermal conduction in 2D heterogeneities with a homogeneous interphase

X.Y. Qu, C.Y. Dong *, Y. Bai, Y.P. Gong

Department of Mechanics, School of Aerospace Engineering, Beijing Institute of Technology, Beijing 100081, China

ARTICLE INFO

Article history:
Received 14 March 2017
Received in revised form 6 September 2017

Keywords:
IGABEM
GSCS
Effective thermal conductivity
Homogeneous interphase

ABSTRACT

Based on the generalized self-consistent scheme (GSCS), the isogeometric boundary element method (IGABEM) is used to calculate the effective thermal conductivity of two dimensional (2D) steady state heat conduction heterogeneities with a homogeneous interphase. The heat energy formulation and the boundary integral equations adopted in this paper only contain the temperatures from the inclusion–interphase and interphase–matrix interfaces, respectively, so that the effective thermal conductivity from the generalized self-consistent model with a homogeneous interphase can be conveniently calculated. In numerical implementation, the Non-Uniform Rational B-Splines (NURBS) are employed not only to construct the exact interface shapes but also to approximate the interface temperatures. The results show that the conductivity and the thickness of the homogeneous interphase have great influence on the effective thermal conductivity. Higher interphase thermal conductivity enhances the effective thermal conductivity, whereas thinner thickness of the interphase results in the reduction of the effective thermal conductivity. Numerical examples show that the proposed method works well compared with the conventional quadratic isoparametric boundary element method.

1. Introduction

The effective properties of composite materials have received much attention in recent years [1]. In order to predict the effective properties of composites, several analytical procedures have been proposed such as the self-consistent method (SCM) devised by Hershey [2] and the generalized self-consistent scheme (GSCS) proposed by Christensen and Lo [3]. The main idea of the SCM is to consider the single particle to be embedded in an effective medium of unknown properties. This method presents a reasonable approximation for some kinds of heterogeneous materials. But for the voids, high volume fractions and rigid inclusions, the SCM cannot exactly describe the behavior of composites [4]. The main idea of the GSCS is to assume that the matrix containing the particle is embedded into an effective medium of unknown properties [3]. This approach can yield better results than the SCM [4].

The steady state thermal conduction problems in inhomogeneous medium have been investigated using many analytical methods and numerical methods [5–16]. He et al. [5] studied thermal conductivities of carbon/carbon fiber composites with inhomogeneous interphase by means of the Mori–Tanaka mean-field concept. Chen and Jiang [11] applied the generalized

* Corresponding author.
E-mail address: cydong@bit.edu.cn (C.Y. Dong).

https://doi.org/10.1016/j.cam.2018.04.053
0377-0427/

self-consistent method and complex variable technology to study the thermal conductivity of fiber reinforced composites with an inhomogeneous interphase. Hatta and Taya [14] studied the heat energy formulation from equivalent inclusion method containing domain integrals which cannot be analytically calculated for complex shaped inhomogeneities. These domain integrals can be obtained using numerical methods, e.g. the finite element method [17]. In order to avoid the appearance of the domain integrals, one can use the similar method from Christensen [18] for the elasticity problems to obtain the heat energy formulation of steady state heat conduction inhomogeneous problems which only contains the interface integrals. But the obtained formulation needs to compute the temperature and heat flux on the inclusion–matrix interfaces in advance. Based on Hatta and Taya's method [14] and Christensen's method [18], Dong [19] presented a heat energy formulation which only contains the temperature on the inclusion–matrix interfaces. This heat energy formulation has been used to study effective thermal conductivities of 2D and 3D steady state heat conduction heterogeneous media [19,20] which only contained some simply shaped inclusions.

The isogeometric analysis (IGA) presented by Hughes et al. [21] has been used to study various problems, e.g. structural and vibration analysis [22], shape optimization [23] and effective elastic property of 2D elastic heterogeneous medium [24]. The IGA establishes a direct link between the computer aided design (CAD) and the finite element method (FEM) or the boundary element method (BEM) [21–24]. The NURBS-based isogeometric analysis possesses the tremendous computational advantages, i.e. high smoothness, than the standard FEM with simple polynomial shape functions. Aimi et al. [25] applied the isogeometric symmetric Galerkin boundary element method (SGBEM) to solve 2D boundary value problems for the Laplace equation and compared the performances of such approach with standard SGBEM and curvilinear SGBEM. In this paper, the GSCS-based IGABEM is presented to investigate effective thermal conductivity of 2D steady state heat conduction composites with complex shaped interphase. In order to verify the GSCS-based IGABEM implementation, convergence studies are shown and numerical results are compared with those from the analytical solutions and the conventional quadratic isoparametric BEM.

2. Basic formulations

2.1. Problem description

Fig. 1 shows a GSCS model with three complex shaped interfaces where Γ_1, Γ_2 and Γ_3 denote the inclusion–interphase interface, the interphase–original matrix interface and the original matrix–effective matrix interface, respectively. The symbols k_M, k_G, k_I and k_E indicate the thermal conduction coefficients of the original matrix, interphase, inclusion and effective matrix, respectively. The q_x^0 and q_y^0 are the heat fluxes along x and y axes, respectively.

2.2. Boundary integral equations

Following Dong [20], we can have the following integral equations

(1) for the source point P on the interface Γ_1,

$$\left(\frac{k_G c_G(P)+k_I c_I(P)}{k_E}\right)u_G(P)=u^0(P)-\int_{\Gamma_1}\left(\frac{k_G-k_I}{k_E}\right)T_G(P,q)\,u_G(q)\,d\Gamma -\int_{\Gamma_2}\left(\frac{k_M-k_G}{k_E}\right)T_M(P,q)\,u_M(q)\,d\Gamma-\int_{\Gamma_3}\left(1-\frac{k_M}{k_E}\right)T_E(P,q)\,u_E(q)\,d\Gamma \tag{1a}$$

(2) for the source point P on the boundary Γ_2,

$$\left(\frac{k_M c_M(P)+k_G c_G(P)}{k_E}\right)u_M(P)=u^0(P)-\int_{\Gamma_1}\left(\frac{k_G-k_I}{k_E}\right)T_G(P,q)\,u_G(q)\,d\Gamma -\int_{\Gamma_2}\left(\frac{k_M-k_G}{k_E}\right)T_M(P,q)\,u_M(q)\,d\Gamma-\int_{\Gamma_3}\left(1-\frac{k_M}{k_E}\right)T_E(P,q)\,u_E(q)\,d\Gamma \tag{1b}$$

(3) for the source point P on the boundary Γ_3,

$$\left(c_E(P)+\frac{k_M}{k_E}c_M(P)\right)u_E(P)=u^0(P)-\int_{\Gamma_1}\left(\frac{k_G-k_I}{k_E}\right)T_G(P,q)\,u_G(q)\,d\Gamma -\int_{\Gamma_2}\left(\frac{k_M-k_G}{k_E}\right)T_M(P,q)\,u_M(q)\,d\Gamma-\int_{\Gamma_3}\left(1-\frac{k_M}{k_E}\right)T_E(P,q)\,u_E(q)\,d\Gamma \tag{1c}$$

where the subscripts M, G, I and E indicate the values from the original matrix, interphase, inclusion and effective matrix, respectively. The $c_M(P)$, $c_G(P)$ and $c_I(P)$ are the constants that depend on the geometries on the interfaces Γ_3, Γ_2 and Γ_1, respectively. $u^0(P)$ is the temperature on the source point P for the whole body composed of the effective material under the far field heat fluxes. $u_E(q)$ is the temperature over the field point q along Γ_3. $u_M(q)$ is the temperature over the field

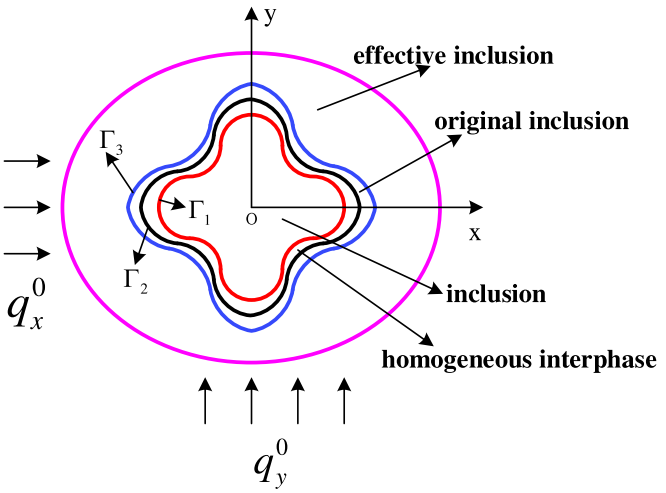

Fig. 1. The GSCS model containing complex shaped inclusion and homogeneous interphase.

point q along Γ_2. $u_G(q)$ is the temperature over the field point q along Γ_1. The symbols T_E, T_M and T_G are the fundamental solutions for 2D steady state systems which have the same form, i.e. [26]:

$$T = \frac{1}{2\pi r}\frac{\partial r}{\partial n} \tag{2}$$

where r is the distance between the source point P and the field point q. $\partial r/\partial n = n_i \partial r/\partial x_i$ where the Einstein sum convention is adopted and n_i is the direction cosine of the normal with respect to x_i.

Based on Eqs. (1a), (1b) and (1c), we can investigate the steady state heterogeneous medium under various remote thermal loadings. The Cauchy singular integrals appearing in Eqs. (1a), (1b) and (1c) can be easily solved by the constant temperature approach which is similar to the rigid displacement method in the elastic problems [26].

Since the effective thermal conductivity is an unknown value in the GSCS, we need to use the iterative method to solve it. The derivatives of Eqs. (1a), (1b) and (1c) with respect to unknown effective thermal conductivity can be written as follows [20]:

$$\begin{aligned}
&\left(\frac{k_G c_G(P) + k_I c_I(P)}{k_E}\right)\dot{u}_G(P) + \int_{\Gamma_1}\left(\frac{k_G - k_I}{k_E}\right)T_G(P,q)\,\dot{u}_G(q)\,d\Gamma \\
&+ \int_{\Gamma_2}\left(\frac{k_M - k_G}{k_E}\right)T_M(P,q)\,\dot{u}_M(q)\,d\Gamma + \int_{\Gamma_3}\left(1 - \frac{k_M}{k_E}\right)T_E(P,q)\,\dot{u}_E(q)\,d\Gamma \\
&- \left(\frac{k_G c_G(P) + k_I c_I(P)}{k_E^2}\right)u_G(P) + \int_{\Gamma_1}\left(-\frac{k_G - k_I}{k_E^2}\right)T_G(P,q)\,u_G(q)\,d\Gamma \\
&+ \int_{\Gamma_2}\left(-\frac{k_M - k_G}{k_E^2}\right)T_M(P,q)\,u_M(q)\,d\Gamma + \int_{\Gamma_3}\left(\frac{k_M}{k_E^2}\right)T_E(P,q)\,u_E(q)\,d\Gamma \\
&= \dot{u}^0(P)
\end{aligned} \tag{3a}$$

and

$$\begin{aligned}
&\left(\frac{k_M c_M(P) + k_G c_G(P)}{k_E}\right)\dot{u}_M(P) + \int_{\Gamma_1}\left(\frac{k_G - k_I}{k_E}\right)T_G(P,q)\,\dot{u}_G(q)\,d\Gamma \\
&+ \int_{\Gamma_2}\left(\frac{k_M - k_G}{k_E}\right)T_M(P,q)\,\dot{u}_M(q)\,d\Gamma + \int_{\Gamma_3}\left(1 - \frac{k_M}{k_E}\right)T_E(P,q)\,\dot{u}_E(q)\,d\Gamma \\
&- \left(\frac{k_M c_M(P) + k_G c_G(P)}{k_E^2}\right)u_M(P) + \int_{\Gamma_1}\left(-\frac{k_G - k_I}{k_E^2}\right)T_G(P,q)\,u_G(q)\,d\Gamma \\
&+ \int_{\Gamma_2}\left(-\frac{k_M - k_G}{k_E^2}\right)T_M(P,q)\,u_M(q)\,d\Gamma + \int_{\Gamma_3}\left(\frac{k_M}{k_E^2}\right)T_E(P,q)\,u_E(q)\,d\Gamma \\
&= \dot{u}^0(P)
\end{aligned} \tag{3b}$$

and

$$\begin{aligned}&\left(c_E(P)+\frac{k_M c_M(P)}{k_E}\right)\dot{u}_E(P)+\int_{\Gamma_1}\left(\frac{k_G-k_I}{k_E}\right)T_G(P,q)\,\dot{u}_G(q)\,d\Gamma\\&+\int_{\Gamma_2}\left(\frac{k_M-k_G}{k_E}\right)T_M(P,q)\,\dot{u}_M(q)\,d\Gamma+\int_{\Gamma_3}\left(1-\frac{k_M}{k_E}\right)T_E(P,q)\,\dot{u}_E(q)\,d\Gamma\\&-\left(\frac{k_M c_M(P)}{k_E^2}\right)u_E(P)+\int_{\Gamma_1}\left(-\frac{k_G-k_I}{k_E^2}\right)T_G(P,q)\,u_G(q)\,d\Gamma\\&+\int_{\Gamma_2}\left(-\frac{k_M-k_G}{k_E^2}\right)T_M(P,q)\,u_M(q)\,d\Gamma+\int_{\Gamma_3}\left(\frac{k_M}{k_E^2}\right)T_E(P,q)\,u_E(q)\,d\Gamma\\&=\dot{u}^0(P)\end{aligned}\tag{3c}$$

where the dot above the temperature u denotes the temperature derivative with respect to k_E, i.e. $\dot{u}=\partial u/\partial k_E$.

Based on the isogeometric analysis which will be presented in the next section and using Eqs. (1a), (1b), (1c), (3a), (3b) and (3c), we can obtain the corresponding matrix equations as follows [20]:

$$\boldsymbol{H}\boldsymbol{u}=\boldsymbol{u}^0\tag{4}$$

and

$$\boldsymbol{H}\dot{\boldsymbol{u}}=\dot{\boldsymbol{u}}^0-\dot{\boldsymbol{H}}\boldsymbol{u}\tag{5}$$

where $\boldsymbol{u}^0$ and $\boldsymbol{u}$ are the known and unknown temperature vectors, respectively. $\dot{\boldsymbol{u}}^0$ and $\dot{\boldsymbol{u}}$ are the corresponding temperature derivatives with respect to the effective thermal conductivity k_E, respectively. $\boldsymbol{H}$ and $\dot{\boldsymbol{H}}$ are the related coefficient matrices from Eqs. (1a), (1b), (1c), (3a), (3b) and (3c), respectively. Once we obtain the interface temperature from Eq. (4), the heat energy of the steady state thermal conduction problem can be obtained as follows [20]:

$$E=E^0+\frac{(k_G-k_I)}{2k_E}\int_{\Gamma_1}n_i q_i^0 u\,d\Gamma+\frac{(k_M-k_G)}{2k_E}\int_{\Gamma_2}n_i q_i^0 u\,d\Gamma+\frac{(k_E-k_M)}{2k_E}\int_{\Gamma_3}n_i q_i^0 u\,d\Gamma\tag{6}$$

where the superscript 0 denotes those values obtained from the homogeneous medium and the heat energy in homogeneous medium composed of the effective material is $E^0=1/2\int_V q_i^0 T_{,i}^0 dV$. One should note that $q_1^0=q_x^0$ and $q_2^0=q_y^0$ (q_x^0 and q_y^0 are shown in Fig. 1). As we have known, the generalized self-consistent scheme should obey the following condition [20]:

$$E=E^0\tag{7}$$

Thus, we can have the following equation [20]:

$$(k_G-k_I)\int_{\Gamma_1}n_i q_i^0 u\,d\Gamma+(k_M-k_G)\int_{\Gamma_2}n_i q_i^0 u\,d\Gamma+(k_E-k_M)\int_{\Gamma_3}n_i q_i^0 u\,d\Gamma=0\tag{8}$$

Now we can use the iterative method for Eqs. (4), (5) and (8) to obtain the effective thermal conductivity.

The computation steps are listed below:

1. Use the NURBS tools to build the NURBS model for the inclusion, interphase and matrix.
2. Input the given values such as temperature and heat flux q_x^0 and q_y^0, and the thermal conduction coefficients k_M, k_G and k_I of matrix, interphase and inclusion, respectively.
3. Give the initial effective thermal conductivity k_E which is taken as $k_E=(k_M+k_G+k_I)/3$.
4. Calculate the solution $\boldsymbol{u}$ of Eq. (4).
5. Calculate the left term from Eq. (8), i.e. $f(k_E)=(k_G-k_I)\int_{\Gamma_1}n_i q_i^0 u\,d\Gamma+(k_M-k_G)\int_{\Gamma_2}n_i q_i^0 u\,d\Gamma+(k_E-k_M)\int_{\Gamma_3}n_i q_i^0 u\,d\Gamma$.
6. If $f(k_E)$ is no more than the given tolerance, i.e. $f(k_E)\le\varepsilon=10^{-3}$, then the k_E is the final effective thermal conductivity so that iteration can be terminated.
7. Otherwise, we need to use Eq. (5) to calculate temperature derivative $\dot{\boldsymbol{u}}$ and the changed value of k_E, i.e. $\Delta k_E=-f(k_E)/\dot{f}(k_E)$ where $\dot{f}(k_E)$ is defined as follows: $\dot{f}(k_E)=(k_G-k_I)\int_{\Gamma_1}n_i q_i^0 \dot{u}\,d\Gamma+(k_M-k_G)\int_{\Gamma_2}n_i q_i^0 \dot{u}\,d\Gamma+(k_E-k_M)\int_{\Gamma_3}n_i q_i^0 \dot{u}\,d\Gamma+\int_{\Gamma_3}n_i q_i^0 u\,d\Gamma$.
8. Modify k_E by $k_E=k_E+\Delta k_E$, then go to 4.

2.3. NURBS and IGABEM

In the isogeometric method, the shape functions that are used to describe the CAD models are also the same functions that are used to approximate the unknown fields in the numerical analysis. Before using the NURBS tools, we should first

use the B-spline tools which can be defined as follows [21,22]:

$$N_{a,0} = \begin{cases} 1 & \xi_a \le \xi < \xi_{a+1} \\ 0 & otherwise \end{cases} \tag{9}$$

and for $p = 1, 2, 3 \ldots$,

$$N_{a,p} = \frac{\xi - \xi_a}{\xi_{a+p} - \xi_a} N_{a,p-1}(\xi) + \frac{\xi_{a+p+1} - \xi}{\xi_{a+p+1} - \xi_{a+1}} N_{a+1,p-1}(\xi). \tag{10}$$

From Eqs. (9) and (10), we can define the B-spline curve as follows:

$$C(\xi) = \sum_{a=1}^{n} N_{a,p}(\xi) P_a \tag{11}$$

where $a = 1, 2, \ldots, n$, n represents the number of control points that are used to define the B-spline, P_a is the ath control point, and $N_{a,p}(\xi)$ is the shape function of the ath control point defined as Eqs. (9) and (10). When the curve is interpolated, one will find that the B-Spline is not exact enough. In order to overcome this case, Hughes and his co-workers [21,22] developed the isogeometric method in which each control point contains an additional weight. Thus, the curve we need can be interpolated exactly.

Now, we can define a NURBS as follows [21,22]:

$$C(\xi) = \sum_{a=1}^{n} R_{a,p}(\xi) P_a \tag{12}$$

where $R_{a,p}(\xi)$ is defined as follows:

$$R_{a,p}(\xi) = \frac{N_{a,p}(\xi) w_a}{\sum_{\hat{a}=1}^{n} N_{\hat{a},p}(\xi) w_{\hat{a}}} \tag{13}$$

where the positive parameters w_a for $a = 1, 2, \ldots, n$ are usually called weights.

Based on the above mentioned equations and following the similar process in Simpson et al.'s work [27,28], we can easily obtain the isogeometric boundary integral equations as follows:

for Eq. (1a),

$$\begin{aligned} &\left(\frac{k_G c_G(x') + k_I c_I(x')}{k_E}\right) \sum_{l=1}^{p+1} N_l^{\bar{e}}\left(\hat{\xi}'\right) u_j^{l\bar{e}} = u^0(x') - \\ &\sum_{e=1}^{N\Gamma_1} \sum_{l=1}^{p+1} \left[\int_{-1}^{1} \left(\frac{k_G - k_I}{k_E}\right) T_G\left(x', x\left(\hat{\xi}\right)\right) N_l^e\left(\hat{\xi}\right) J\left(\hat{\xi}\right) d\hat{\xi}\right] d_j^{le} - \\ &\sum_{e=1}^{N\Gamma_2} \sum_{l=1}^{p+1} \left[\int_{-1}^{1} \left(\frac{k_M - k_G}{k_E}\right) T_M\left(x', x\left(\hat{\xi}\right)\right) N_l^e\left(\hat{\xi}\right) J\left(\hat{\xi}\right) d\hat{\xi}\right] d_j^{le} - \\ &\sum_{e=1}^{N\Gamma_3} \sum_{l=1}^{p+1} \left[\int_{-1}^{1} \left(1 - \frac{k_M}{k_E}\right) T_E\left(x', x\left(\hat{\xi}\right)\right) N_l^e\left(\hat{\xi}\right) J\left(\hat{\xi}\right) d\hat{\xi}\right] d_j^{le} \end{aligned} \tag{14a}$$

and for Eq. (1b),

$$\begin{aligned} &\left(\frac{k_M c_M(x') + k_G c_G(x')}{k_E}\right) \sum_{l=1}^{p+1} N_l^{\bar{e}}\left(\hat{\xi}'\right) u_j^{l\bar{e}} = u^0(x') - \\ &\sum_{e=1}^{N\Gamma_1} \sum_{l=1}^{p+1} \left[\int_{-1}^{1} \left(\frac{k_G - k_I}{k_E}\right) T_G\left(x', x\left(\hat{\xi}\right)\right) N_l^e\left(\hat{\xi}\right) J\left(\hat{\xi}\right) d\hat{\xi}\right] d_j^{le} - \\ &\sum_{e=1}^{N\Gamma_2} \sum_{l=1}^{p+1} \left[\int_{-1}^{1} \left(\frac{k_M - k_G}{k_E}\right) T_M\left(x', x\left(\hat{\xi}\right)\right) N_l^e\left(\hat{\xi}\right) J\left(\hat{\xi}\right) d\hat{\xi}\right] d_j^{le} - \\ &\sum_{e=1}^{N\Gamma_3} \sum_{l=1}^{p+1} \left[\int_{-1}^{1} \left(1 - \frac{k_M}{k_E}\right) T_E\left(x', x\left(\hat{\xi}\right)\right) N_l^e\left(\hat{\xi}\right) J\left(\hat{\xi}\right) d\hat{\xi}\right] d_j^{le} \end{aligned} \tag{14b}$$

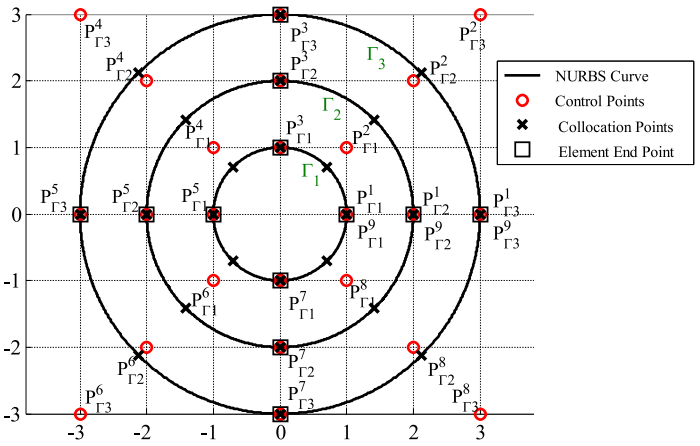

Fig. 2. The isogeometric model of three circle interfaces whose geometry parameters are also used to describe the GSCS effective matrix, interphase and circle inclusion. We use 9 control points to build each interface's coarse model, where the 9th control point is the same as the 1st control point. The knot vector for each interface is $\boldsymbol{U} = [0, 0, 0, 1, 1, 2, 2, 3, 3, 4, 4, 4]$ and the corresponding control points' weight vector is $\boldsymbol{w} = \left[1, \frac{\sqrt{2}}{2}, 1, \frac{\sqrt{2}}{2}, 1, \frac{\sqrt{2}}{2}, 1, \frac{\sqrt{2}}{2}, 1\right]$.

and for Eq. (1c),

$$\begin{aligned}
&\left(c_E\left(x'\right)+\frac{k_M}{k_E}c_M\left(x'\right)\right)\sum_{l=1}^{p+1}N_l^{\bar{e}}\left(\hat{\xi}'\right)u_j^{l\bar{e}}=u^0\left(x'\right)-\\
&\sum_{e=1}^{N\Gamma_1}\sum_{l=1}^{p+1}\left[\int_{-1}^{1}\left(\frac{k_G-k_I}{k_E}\right)T_G\left(x',x\left(\hat{\xi}\right)\right)N_l^e\left(\hat{\xi}\right)J\left(\hat{\xi}\right)d\hat{\xi}\right]d_j^{le}-\\
&\sum_{e=1}^{N\Gamma_2}\sum_{l=1}^{p+1}\left[\int_{-1}^{1}\left(\frac{k_M-k_G}{k_E}\right)T_M\left(x',x\left(\hat{\xi}\right)\right)N_l^e\left(\hat{\xi}\right)J\left(\hat{\xi}\right)d\hat{\xi}\right]d_j^{le}-\\
&\sum_{e=1}^{N\Gamma_3}\sum_{l=1}^{p+1}\left[\int_{-1}^{1}\left(1-\frac{k_M}{k_E}\right)T_E\left(x',x\left(\hat{\xi}\right)\right)N_l^e\left(\hat{\xi}\right)J\left(\hat{\xi}\right)d\hat{\xi}\right]d_j^{le}.
\end{aligned}\tag{14c}$$

For Eqs. (3a), (3b) and (3c), we can have the isogeometric boundary integral equations as follows:
for Eq. (3a),

$$\begin{aligned}
&\left(\frac{k_Gc_G\left(x'\right)+k_Ic_I\left(x'\right)}{k_E}\right)\sum_{l=1}^{p+1}N_l^{\bar{e}}\left(\hat{\xi}'\right)\dot{u}_j^{l\bar{e}}+\\
&\sum_{e=1}^{N\Gamma_1}\sum_{l=1}^{p+1}\left[\int_{-1}^{1}\left(\frac{k_G-k_I}{k_E}\right)T_G\left(x',x\left(\hat{\xi}\right)\right)N_l^e\left(\hat{\xi}\right)J\left(\hat{\xi}\right)d\hat{\xi}\right]\dot{d}_j^{le}+\\
&\sum_{e=1}^{N\Gamma_2}\sum_{l=1}^{p+1}\left[\int_{-1}^{1}\left(\frac{k_M-k_G}{k_E}\right)T_M\left(x',x\left(\hat{\xi}\right)\right)N_l^e\left(\hat{\xi}\right)J\left(\hat{\xi}\right)d\hat{\xi}\right]\dot{d}_j^{le}+\\
&\sum_{e=1}^{N\Gamma_3}\sum_{l=1}^{p+1}\left[\int_{-1}^{1}\left(1-\frac{k_M}{k_E}\right)T_E\left(x',x\left(\hat{\xi}\right)\right)N_l^e\left(\hat{\xi}\right)J\left(\hat{\xi}\right)d\hat{\xi}\right]\dot{d}_j^{le}-\\
&\left(\frac{k_Gc_G\left(x'\right)+k_Ic_I\left(x'\right)}{k_E^2}\right)\sum_{l=1}^{p+1}N_l^{\bar{e}}\left(\hat{\xi}'\right)u_j^{l\bar{e}}+\\
&\sum_{e=1}^{N\Gamma_1}\sum_{l=1}^{p+1}\left[\int_{-1}^{1}\left(-\frac{k_G-k_I}{k_E^2}\right)T_G\left(x',x\left(\hat{\xi}\right)\right)N_l^e\left(\hat{\xi}\right)J\left(\hat{\xi}\right)d\hat{\xi}\right]d_j^{le}+\\
&\sum_{e=1}^{N\Gamma_2}\sum_{l=1}^{p+1}\left[\int_{-1}^{1}\left(-\frac{k_M-k_G}{k_E^2}\right)T_M\left(x',x\left(\hat{\xi}\right)\right)N_l^e\left(\hat{\xi}\right)J\left(\hat{\xi}\right)d\hat{\xi}\right]d_j^{le}+\\
&\sum_{e=1}^{N\Gamma_3}\sum_{l=1}^{p+1}\left[\int_{-1}^{1}\left(\frac{k_M}{k_E^2}\right)T_E\left(x',x\left(\hat{\xi}\right)\right)N_l^e\left(\hat{\xi}\right)J\left(\hat{\xi}\right)d\hat{\xi}\right]d_j^{le}\\
&=\dot{u}^0\left(x'\right)
\end{aligned}\tag{15a}$$

and for Eq. (3b),

$$\begin{aligned}
&\left(\frac{k_M c_M\left(x'\right)+k_G c_G\left(x'\right)}{k_E}\right)\sum_{l=1}^{p+1}N_l^{\bar{e}}\left(\hat{\xi}'\right)\dot{u}_j^{l\bar{e}}+\\
&\sum_{e=1}^{N\Gamma_1}\sum_{l=1}^{p+1}\left[\int_{-1}^{1}\left(\frac{k_G-k_I}{k_E}\right)T_G\left(x',x\left(\hat{\xi}\right)\right)N_l^e\left(\hat{\xi}\right)J\left(\hat{\xi}\right)d\hat{\xi}\right]\dot{d}_j^{le}+\\
&\sum_{e=1}^{N\Gamma_2}\sum_{l=1}^{p+1}\left[\int_{-1}^{1}\left(\frac{k_M-k_G}{k_E}\right)T_M\left(x',x\left(\hat{\xi}\right)\right)N_l^e\left(\hat{\xi}\right)J\left(\hat{\xi}\right)d\hat{\xi}\right]\dot{d}_j^{le}+\\
&\sum_{e=1}^{N\Gamma_3}\sum_{l=1}^{p+1}\left[\int_{-1}^{1}\left(1-\frac{k_M}{k_E}\right)T_E\left(x',x\left(\hat{\xi}\right)\right)N_l^e\left(\hat{\xi}\right)J\left(\hat{\xi}\right)d\hat{\xi}\right]\dot{d}_j^{le}-\\
&\left(\frac{k_M c_M\left(x'\right)+k_G c_G\left(x'\right)}{k_E^2}\right)\sum_{l=1}^{p+1}N_l^{\bar{e}}\left(\hat{\xi}'\right)u_j^{l\bar{e}}+\\
&\sum_{e=1}^{N\Gamma_1}\sum_{l=1}^{p+1}\left[\int_{-1}^{1}\left(-\frac{k_G-k_I}{k_E^2}\right)T_G\left(x',x\left(\hat{\xi}\right)\right)N_l^e\left(\hat{\xi}\right)J\left(\hat{\xi}\right)d\hat{\xi}\right]d_j^{le}+\\
&\sum_{e=1}^{N\Gamma_2}\sum_{l=1}^{p+1}\left[\int_{-1}^{1}\left(-\frac{k_M-k_G}{k_E^2}\right)T_M\left(x',x\left(\hat{\xi}\right)\right)N_l^e\left(\hat{\xi}\right)J\left(\hat{\xi}\right)d\hat{\xi}\right]d_j^{le}+\\
&\sum_{e=1}^{N\Gamma_3}\sum_{l=1}^{p+1}\left[\int_{-1}^{1}\left(\frac{k_M}{k_E^2}\right)T_E\left(x',x\left(\hat{\xi}\right)\right)N_l^e\left(\hat{\xi}\right)J\left(\hat{\xi}\right)d\hat{\xi}\right]d_j^{le}\\
&=\dot{u}^0\left(x'\right)
\end{aligned}\tag{15b}$$

and for Eq. (3c),

$$\begin{aligned}
&\left(c_E\left(x'\right)+\frac{k_M c_M\left(x'\right)}{k_E}\right)\sum_{l=1}^{p+1}N_l^{\bar{e}}\left(\hat{\xi}'\right)\dot{u}_j^{l\bar{e}}+\\
&\sum_{e=1}^{N\Gamma_1}\sum_{l=1}^{p+1}\left[\int_{-1}^{1}\left(\frac{k_G-k_I}{k_E}\right)T_G\left(x',x\left(\hat{\xi}\right)\right)N_l^e\left(\hat{\xi}\right)J\left(\hat{\xi}\right)d\hat{\xi}\right]\dot{d}_j^{le}+\\
&\sum_{e=1}^{N\Gamma_2}\sum_{l=1}^{p+1}\left[\int_{-1}^{1}\left(\frac{k_M-k_G}{k_E}\right)T_M\left(x',x\left(\hat{\xi}\right)\right)N_l^e\left(\hat{\xi}\right)J\left(\hat{\xi}\right)d\hat{\xi}\right]\dot{d}_j^{le}+\\
&\sum_{e=1}^{N\Gamma_3}\sum_{l=1}^{p+1}\left[\int_{-1}^{1}\left(1-\frac{k_M}{k_E}\right)T_E\left(x',x\left(\hat{\xi}\right)\right)N_l^e\left(\hat{\xi}\right)J\left(\hat{\xi}\right)d\hat{\xi}\right]\dot{d}_j^{le}-\\
&\left(\frac{k_M c_M\left(x'\right)}{k_E^2}\right)\sum_{l=1}^{p+1}N_l^{\bar{e}}\left(\hat{\xi}'\right)u_j^{l\bar{e}}+\\
&\sum_{e=1}^{N\Gamma_1}\sum_{l=1}^{p+1}\left[\int_{-1}^{1}\left(-\frac{k_G-k_I}{k_E^2}\right)T_G\left(x',x\left(\hat{\xi}\right)\right)N_l^e\left(\hat{\xi}\right)J\left(\hat{\xi}\right)d\hat{\xi}\right]d_j^{le}+\\
&\sum_{e=1}^{N\Gamma_2}\sum_{l=1}^{p+1}\left[\int_{-1}^{1}\left(-\frac{k_M-k_G}{k_E^2}\right)T_M\left(x',x\left(\hat{\xi}\right)\right)N_l^e\left(\hat{\xi}\right)J\left(\hat{\xi}\right)d\hat{\xi}\right]d_j^{le}+\\
&\sum_{e=1}^{N\Gamma_3}\sum_{l=1}^{p+1}\left[\int_{-1}^{1}\left(\frac{k_M}{k_E^2}\right)T_E\left(x',x\left(\hat{\xi}\right)\right)N_l^e\left(\hat{\xi}\right)J\left(\hat{\xi}\right)d\hat{\xi}\right]d_j^{le}\\
&=\dot{u}^0\left(x'\right)
\end{aligned}\tag{15c}$$

where $\hat{\xi}'$ represents the nodal parameter of the knot vector that corresponds to the source point x'. $x\left(\hat{\xi}\right)$ denotes the field point where $\hat{\xi}\in[-1,1]$ represents the parameter for the Gauss integral. The symbol l is a local node number. The superscripts e and $\bar{e}$ represent the element which varies from 1 to N_e and the element at which the source point locates, respectively. $p=1$ is for the linear element, whereas $p=2$ is for the quadratic element. N_l^e is the shape function of lth node which locates at the element e. $J=\frac{d\Gamma}{d\hat{\xi}}$ is the Jacobian of transformation. $N\Gamma_1$, $N\Gamma_2$ and $N\Gamma_3$ represent the element numbers of the interfaces Γ_1, Γ_2 and Γ_3, respectively. In the IGABEM, the control points are not always located on the real boundary and the NURBS basis functions do not necessarily obey the Kronecker-Delta property, so d_i^{le} and $\dot{d}_i^{le}$ are just the coefficients

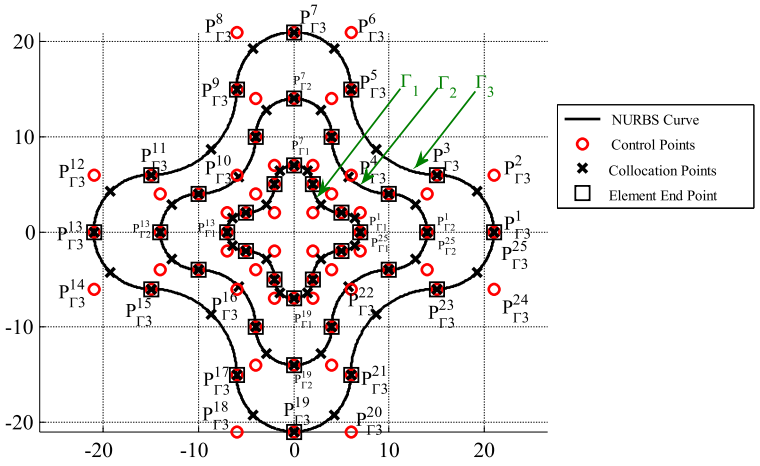

Fig. 3. The first isogeometric model with complex shaped interfaces which are used to describe the GSCS effective matrix, interphase and inclusion. We use 25 control points to build this coarse model. The knot vector and weight vector for each interface are given as $\boldsymbol{U} = [0, 0, 0, 1, 1, 2, 2, 3, 3, 4, 4, 5, 5, 6, 6, 7, 7, 8, 8, 9, 9, 10, 10, 11, 11, 12, 12, 12]$ and $\boldsymbol{w} = \left[1, \frac{\sqrt{2}}{2}, 1, \frac{\sqrt{2}}{2}, 1, \frac{\sqrt{2}}{2}, 1, \frac{\sqrt{2}}{2}, 1, \frac{\sqrt{2}}{2}, 1, \frac{\sqrt{2}}{2}, 1, \frac{\sqrt{2}}{2}, 1, \frac{\sqrt{2}}{2}, 1, \frac{\sqrt{2}}{2}, 1, \frac{\sqrt{2}}{2}, 1, \frac{\sqrt{2}}{2}, 1, \frac{\sqrt{2}}{2}, 1\right]$, respectively.

of temperature and its derivative, respectively. The true temperature and its derivative can be interpolated as follows:

$$\begin{cases} u_j\left(x'\right) = \sum_{l=1}^{p+1} N_l^{\bar{e}}\left(\hat{\xi}'\right) d_j^{l\bar{e}} \\ \dot{u}_j\left(x'\right) = \sum_{l=1}^{p+1} N_l^{\bar{e}}\left(\hat{\xi}'\right) \dot{d}_j^{l\bar{e}} \end{cases} \tag{16}$$

Now based on Eqs. (14a), (14b), (14c), (15a), (15b) and (15c), we can carry out the IGABEM analysis for the 2D steady state heat conduction problems. The isogeometric GSCS models will be presented in next section.

3. Isogeometric models

We use the isogeometric method to build one circular inclusion model and three different inclusion models with complex shaped interfaces. All these models are initially the coarse control meshes. Following these initial models, we can adopt the isogeometric refinement algorithm to improve these models. All GSCS models are shown in Figs. 2–5, respectively. In all the models, $P^i_{\Gamma_1}$, $P^i_{\Gamma_2}$ and $P^i_{\Gamma_3}$ represent the ith control points that belong to the interfaces Γ_1, Γ_2 and Γ_3, respectively.

4. Numerical examples

The formulations presented in the previous sections have been programmed by Fortran 95 and the corresponding code has been validated through the solutions available. The present results from an infinite plane with a circular inclusion under a remote thermal loading are in good agreement with the analytical solutions [16] and the sub-domain boundary element (Sub-BEM) solutions [28]. Therefore, we will only analyze a couple of new inhomogeneous problems with circular and complex shaped interphases in the following.

4.1. GSCS model with circular interfaces (Fig. 2)

The GSCS model with circle inclusion and homogeneous interphase is shown in Fig. 2. The composite is under the remote heat fluxes, i.e. $q_x^0 = 1.0$ and $q_y^0 = 2.0$ which are also the same as for the other GSCS models. The reference temperature is taken as 100° C. Four different materials for all the GSCS models are also taken into consideration, i.e. Case I: $k_M = 1.0, k_I = 0.5, k_G = 0.5$; Case II: $k_M = 1.0, k_I = 0.5, k_G = 0.7$; Case III: $k_M = 1.0, k_I = 2.0, k_G = 1.5$ and Case IV: $k_M = 1.0, k_I = 2.0, k_G = 2.0$. The k_M, k_G and k_I are the thermal conductivities of matrix, interphase and inclusion, respectively. Fig. 6a1 shows the results of analytical solutions [11], Sub-BEM [28] and IGABEM, where Case I–Case IV are applied under the same heat flux that has been mentioned as before. One can observe that compared with Sub-BEM [28], the IGABEM produces more accurate results using fewer elements. The reason is in the fact that there is no geometrical error in the analysis of the IGABEM.

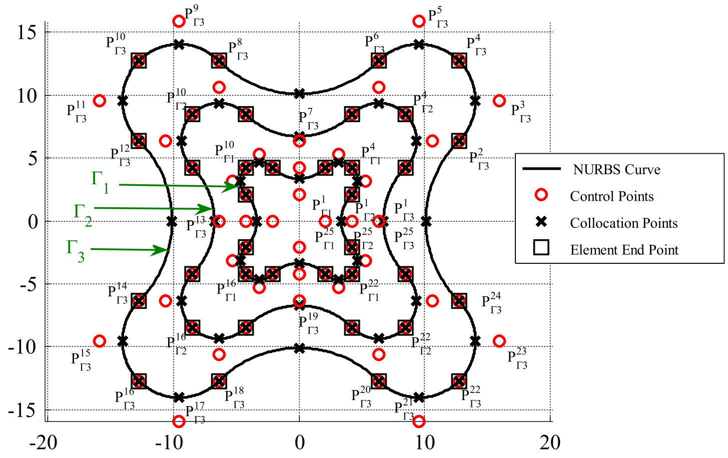

Fig. 4. The second isogeometric model with complex shaped interfaces which are used to describe the GSCS effective matrix, interphase and inclusion. We use 25 control points to build this coarse model. The knot vector and weight vector for each interface are given as: $\boldsymbol{U} = [0, 0, 0, 1, 1, 2, 2, 3, 3, 4, 4, 5, 5, 6, 6, 7, 7, 8, 8, 9, 9, 10, 10, 11, 11, 12, 12, 12]$ and $\boldsymbol{w} = \left[1, \frac{\sqrt{2}}{2}, 1, \frac{\sqrt{2}}{2}, 1, \frac{\sqrt{2}}{2}, 1, \frac{\sqrt{2}}{2}, 1, \frac{\sqrt{2}}{2}, 1, \frac{\sqrt{2}}{2}, 1, \frac{\sqrt{2}}{2}, 1, \frac{\sqrt{2}}{2}, 1, \frac{\sqrt{2}}{2}, 1, \frac{\sqrt{2}}{2}, 1, \frac{\sqrt{2}}{2}, 1, \frac{\sqrt{2}}{2}, 1\right]$, respectively.

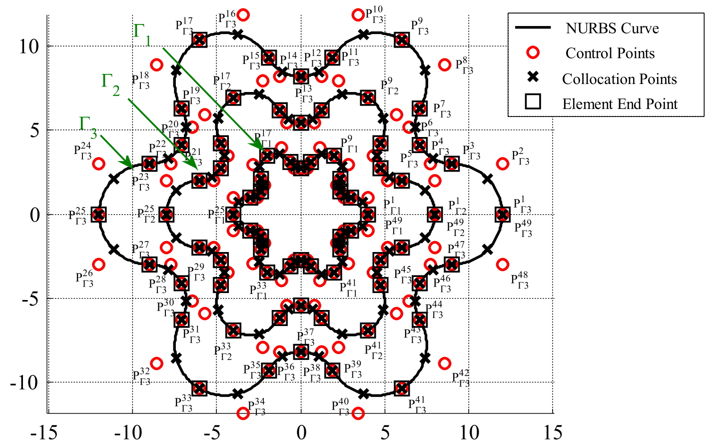

Fig. 5. Third isogeometric model with complex shaped interfaces which are used to describe the GSCS effective matrix, interphase and inclusion. We use 49 control points to build this model. The knot vector and weight vector for each interface are respectively given as $\boldsymbol{U} = [0, 0, 0, 1, 1, 2, 2, 3, 3, 4, 4, 5, 5, 6, 6, 7, 7, 8, 8, 9, 9, 10, 10, 11, 11, 12, 12, 13, 13, 14, 14, 15, 15, 16, 16, 17, 17, 18, 18, 19, 19, 20, 20, 21, 21, 22, 22, 23, 23, 24, 24, 24]$ and $\boldsymbol{w} = [1, \frac{\sqrt{2}}{2}, 1, \frac{\sqrt{3}}{2}, 1, \frac{\sqrt{3}}{2}, 1, \frac{\sqrt{2}}{2}, 1, \frac{\sqrt{2}}{2}, 1, \frac{\sqrt{3}}{2}, 1, \frac{\sqrt{3}}{2}, 1, \frac{\sqrt{2}}{2}, 1, \frac{\sqrt{2}}{2}, 1, \frac{\sqrt{3}}{2}, 1, \frac{\sqrt{3}}{2}, 1, \frac{\sqrt{2}}{2}, 1, \frac{\sqrt{2}}{2}, 1, \frac{\sqrt{3}}{2}, 1, \frac{\sqrt{3}}{2}, 1, \frac{\sqrt{2}}{2}, 1, \frac{\sqrt{2}}{2}, 1, \frac{\sqrt{3}}{2}, 1, \frac{\sqrt{3}}{2}, 1, \frac{\sqrt{2}}{2}, 1, \frac{\sqrt{2}}{2}, 1, \frac{\sqrt{3}}{2}, 1, \frac{\sqrt{3}}{2}, 1, \frac{\sqrt{2}}{2}, 1]$, respectively.

When the interphase is not considered, the present GSCS models reduce to the conventional GSCS models which have been widely investigated. Here, two different materials for all the conventional GSCS models in the following examples are also taken into consideration, i.e. Case V: $k_M = 1.0$, $k_I = 0.5$ and Case VI: $k_M = 1.0$, $k_I = 2.0$. These cases are applied under the same heat flux that has mentioned as before. Fig. 6a2 shows the results from analytical solutions [11], Sub-BEM [28] and IGABEM in the two cases without interphases. Similar to the cases with interphases, the IGABEM also shows more accurate results using fewer elements compared with the Sub-BEM [28].

In order to check the convergence of the IGABEM, various refinements are given to calculate the effective thermal conductivities. Here, one should notice that refinement=m ($m = 1, 2, \ldots, 10$) denotes that each knot vector is refined with $Ne = 4 * m$ (m represents the refinement number, and $m = 1$ means that we use the initial coarse model and the four elements ($Ne = 4$) for each interface). The convergence property of the Sub-BEM is studied using various element numbers on each interface, i.e. $Ne = 4 * n$ ($n = 1, 2, \ldots, 18$). Figs. 6b and 6d show the convergence results of the IGABEM under different refinements for $k_I/k_M = 0.5$ and 2.0, respectively. Figs. 6c and 6e show the convergence results of the Sub-BEM under different element numbers for $k_I/k_M = 0.5$ and 2.0, respectively. Figs. 6b and 6e indicate that the results obtained by the IGABEM and the Sub-BEM are convergent and reliable, and the IGABEM is more efficient and accurate than the Sub-BEM since there is no geometric error in the IGABEM.

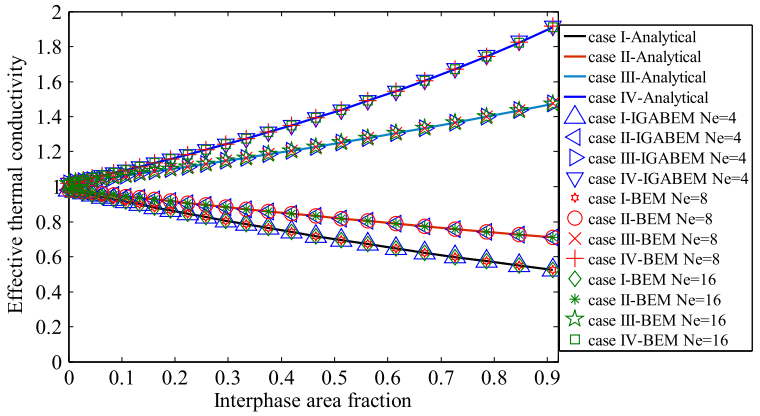

Fig. 6a1. The effective thermal conductivities of Case I to Case IV, which are obtained by the analytical method, Sub-BEM and IGABEM. The interphase area fraction represents the area fraction of 2D case, i.e. $(Area_{\Gamma_2} - Area_{\Gamma_1})/Area_{\Gamma_3}$, where $Area_{\Gamma_1}$, $Area_{\Gamma_2}$ and $Area_{\Gamma_3}$ represent the areas surrounded by the interfaces Γ_1, Γ_2 and Γ_3, respectively.

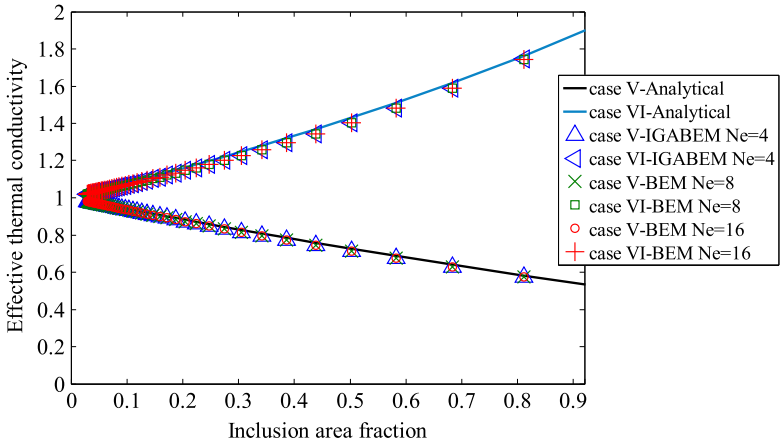

Fig. 6a2. The effective thermal conductivities of Case V to Case VI for no interphase, which are obtained by the analytical method, Sub-BEM and IGABEM. The inclusion area fraction represents the inclusion area fraction of 2D case and is defined as $Area_{\Gamma_1}/Area_{\Gamma_3}$, where $Area_{\Gamma_1}$ and $Area_{\Gamma_3}$ represent the areas surrounded by the interfaces Γ_1 and Γ_3, respectively.

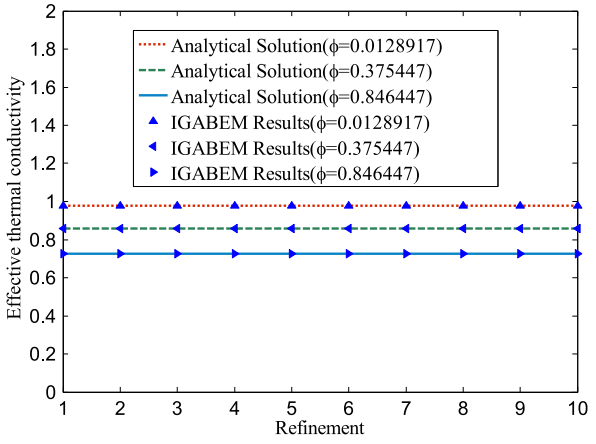

Fig. 6b. The IGABEM convergence test for $k_I/k_M < 1$, where we take $k_I = 0.5$, $K_G = 0.7$ and use three different interphase area fraction values to obtain the convergent results under different refinements.

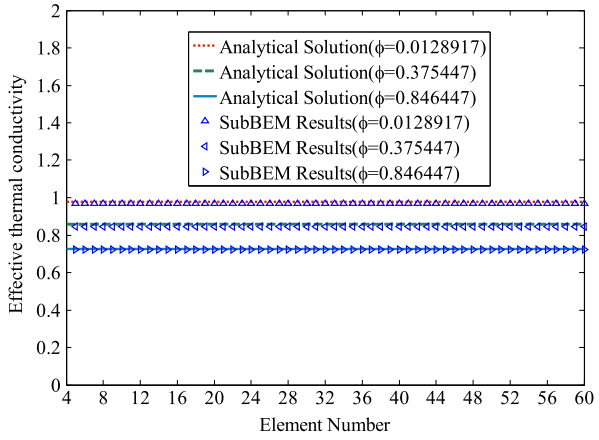

Fig. 6c. The Sub-BEM convergence test for $k_I/k_M < 1$, where we take $k_I = 0.5$, $K_G = 0.7$ and use three different interphase area fraction values to obtain the convergent results under different element numbers.

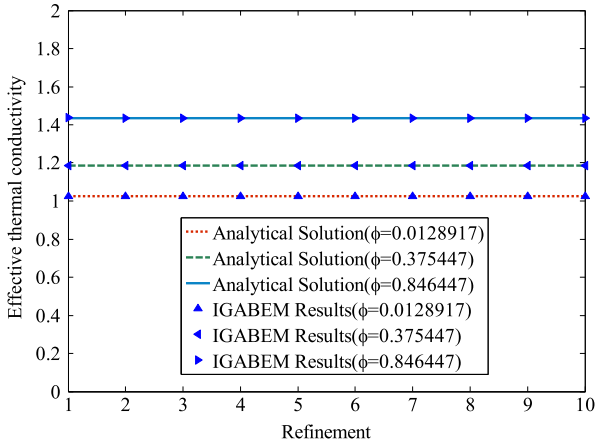

Fig. 6d. The IGABEM convergence test for $k_I/k_M > 1$, where we take $k_I = 2.0$, $K_G = 1.5$ and use three different interphase area fraction values to obtain the convergent results under different refinements.

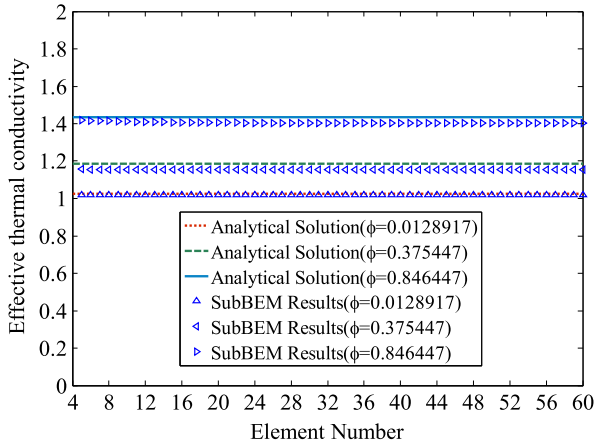

Fig. 6e. The Sub-BEM convergent test for $k_I/k_M > 1$ case, where we take $k_I = 2.0$, $K_G = 1.5$ and use three different interphase area fraction values to obtain the convergent results under different element numbers.

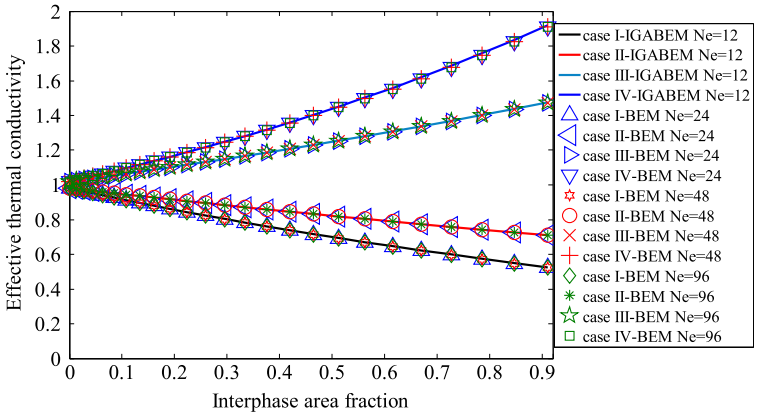

Fig. 7a. The effective thermal conductivities of the first complex GSCS model from Case I to Case IV, which are obtained by the Sub-BEM and IGABEM, respectively. The interphase area fraction represents the area fraction of 2D case.

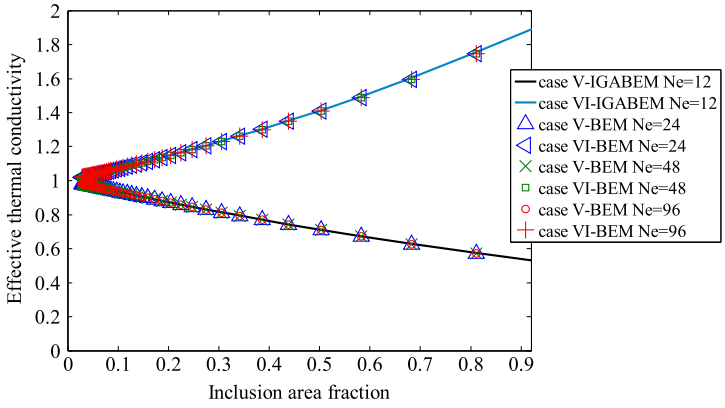

Fig. 7b. The effective thermal conductivities of the first complex GSCS model without interphase from Case V to Case VI, which are obtained by the Sub-BEM and IGABEM, respectively. The inclusion area fraction represents the inclusion area fraction of 2D case. Two different materials for all the GSCS models are also taken into consideration, i.e. Case V: $k_M = 1.0$, $k_I = 0.5$ and Case VI: $k_M = 1.0$, $k_I = 2.0$.

4.2. The GSCS models with complex shaped interphase

Based on the fact that the IGABEM's results are in good agreement with those from other methods such as the Sub-BEM and analytical method [16], we consider three different complex GSCS models as shown in Figs. 3–5. The material properties are the same for four different material cases and the remote heat fluxes are also the same as those in Section 4.1. In order to obtain the correct results, we use different element numbers in the Sub-BEM, which are refined from the coarse meshes to the fine meshes, to obtain the convergence results. But for the IGABEM, only 12 elements are used. From Figs. 7a–9b, one can observe that good agreement from the Sub-BEM with different element numbers and the IGABEM has been obtained. For a high K_G, the homogeneous interphase enhances the effective thermal conductivity. Otherwise, it can reduce the effective thermal conductivity. The enhancement of the effective conductivity is also reliant to the homogeneous interphase's thickness. As the homogeneous interphase becomes thin, the enhancement of the effective conductivity is reduced. Fig. 10a shows that the effective thermal conductivity of these three different inclusions with complex shapes have almost the same results. Fig. 10b displays the effective thermal conductivities of three different complex GSCS models from Case V to Case VI, which are obtained by the IGABEM in the case of the idealized zero thickness homogeneous interphase, respectively. We can find that the complex geometries of the GSCS model have less effect on the effective thermal conductivity.

5. Conclusion

The effective thermal conductivity is an important property in composites. Compared with the geometry of the inclusion, the area fraction has more important effect on this property. With the greater ratio of the thermal conductivity of the homogeneous interphase and matrix, the homogeneous interphase's effect on the effective thermal conductivity of the composites is greater. Otherwise, the effective thermal conductivity is reduced. And as the homogeneous interphase is

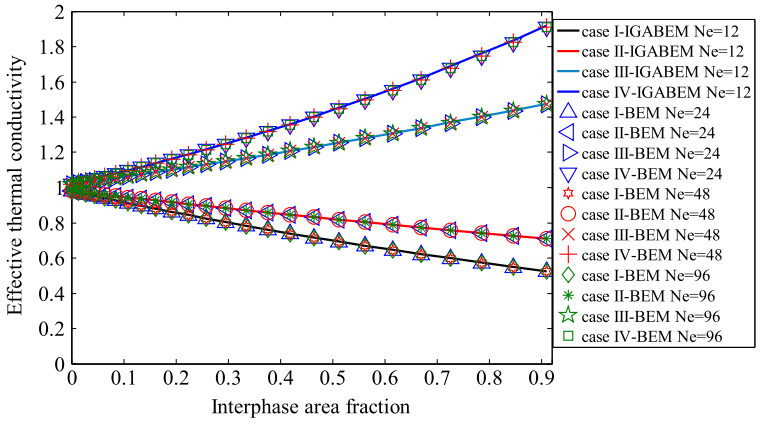

Fig. 8a. The effective thermal conductivities of the second complex GSCS model from Case I to Case IV, which are obtained by the Sub-BEM and IGABEM, respectively. The interphase area fraction represents the area fraction of 2D case.

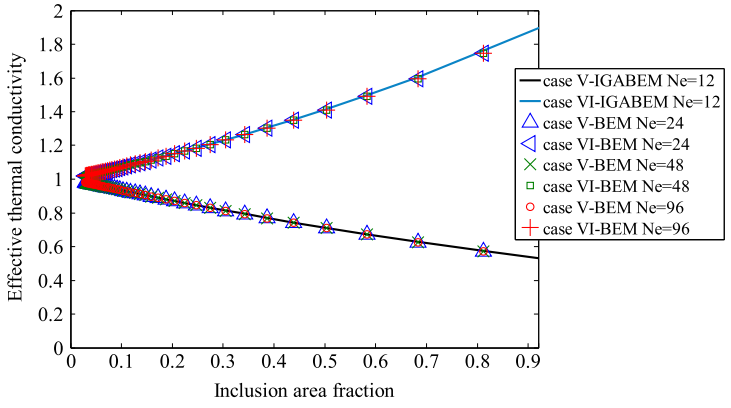

Fig. 8b. The effective thermal conductivities of the second complex GSCS model without interphase from Case V to Case VI, which are obtained by the Sub-BEM and IGABEM, respectively. The inclusion area fraction represents the inclusion area fraction of 2D case.

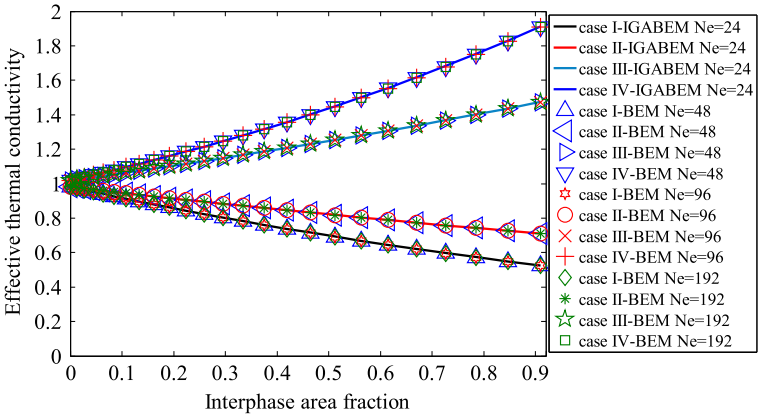

Fig. 9a. The effective thermal conductivities of the third complex GSCS model from Case I to Case IV, which are obtained by the Sub-BEM and IGABEM, respectively. The interphase area fraction represents the area fraction of 2D case.

thickened, the enhancement of the effective conductivity is increased. The isogeometric analysis is a useful tool and a good alternative to investigate the heterogeneous problems with complex shaped inclusions. The IGABEM is an effective numerical method that can allow us directly carry out the analysis after we establish exact geometrical model. Compared with the Sub-BEM, the IGABEM can use much less degrees of freedom to obtain the same good results. The present work can be a reference for other numerical methods which are used to study the steady state heat conduction problems.

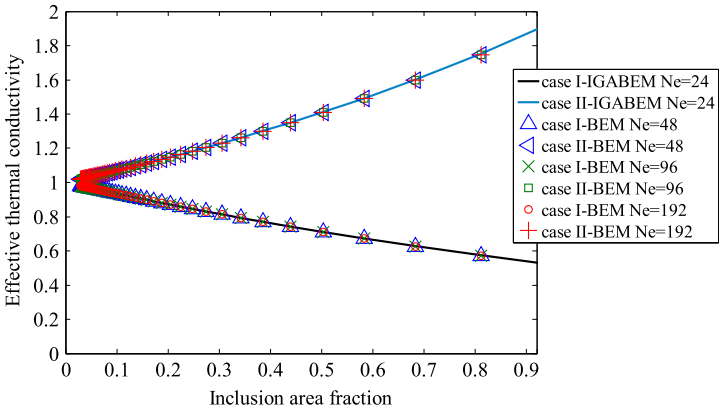

Fig. 9b. The effective thermal conductivities of the third complex GSCS model without interphase from Case V to Case VI, which are obtained by the Sub-BEM and IGABEM, respectively. The inclusion area fraction represents the inclusion area fraction of 2D case.

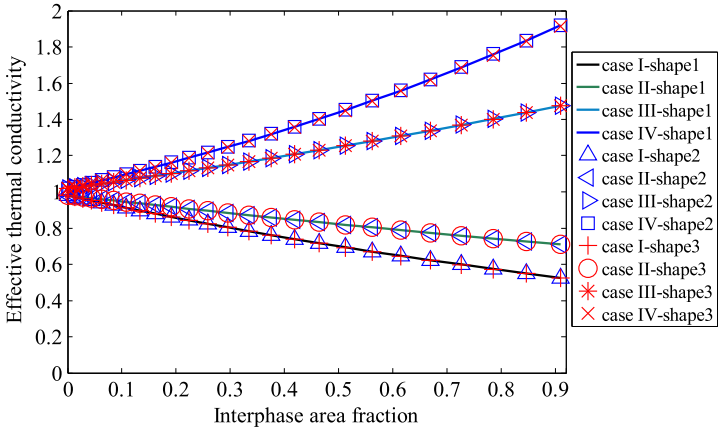

Fig. 10a. The effective thermal conductivities of three different complex GSCS models from Case I to Case IV, which are obtained by the IGABEM, respectively. The interphase area fraction represents the area fraction of 2D case. Shape1 refers to the first complex shape which is shown in Fig. 3. Shape2 refers to the second complex shape which is shown in Fig. 4. Shape3 refers to the third complex shape which is shown in Fig. 5.

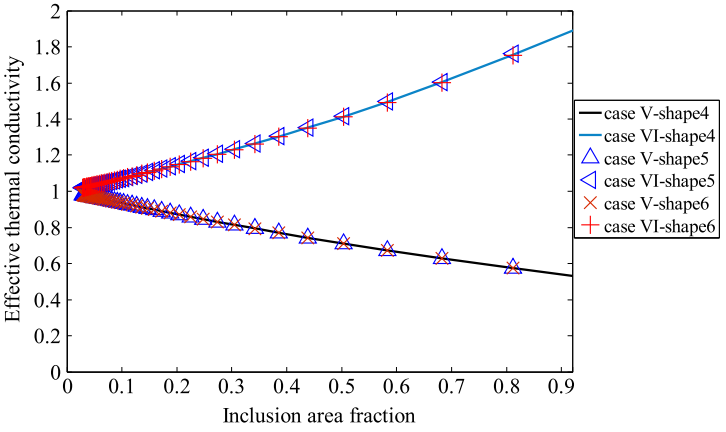

Fig. 10b. The effective thermal conductivities of three different complex GSCS models from Case V to Case VI, which are obtained by the IGABEM in the case of the idealized zero thickness homogeneous interphase, respectively. The inclusion area fraction represents the inclusion area fraction of 2D case. Shape4 refers to the first complex shape without homogeneous interphase which is shown in Fig. 3. Shape5 refers to the second complex shape without homogeneous interphase which is shown in Fig. 4. Shape6 refers to the third complex shape without homogeneous interphase which is shown in Fig. 5.

Acknowledgment

The research is supported by the National Natural Science Foundation of China (11672038, 11272054).

References

[1] G.J. Rodin, G.J. Weng, On reflected interactions in elastic solids containing inhomogeneities, J. Mech. Phys. Solids 68 (1) (2014) 197–209.
[2] A.V. Hershey, The elasticity of an isotropic aggregate of anisotropic cubic crystals, J. Appl. Mech Trans. ASME 21 (1954) 236–240.
[3] R.M. Christensen, K.H. Lo, Solutions for effective shear properties in three phase sphere and kcylinder models, J. Mech. Phys. Solids 27 (4) (1979) 315–330.
[4] J. Aboudi, S.M. Arnold, B.A. Bednarcyk, Micromechanics of Composite Materials-a Generalized Multiscale Analysis Approach, Elsevier, Amsterdam, 2013.
[5] L.H. He, Z.Q. Cheng, R.H. Liu, Investigation on the effective conductivities of carbon/carbon fiber composites with inhomogeneous interphase, Appl. Math. Mech. 3 (1997) 193–201.
[6] Y.M. Lee, R.B. Yang, S.S. Gau, A generalized self-consistent method for calculation of effective thermal conductivity of composites with interfacial contact conductance, Int. Commun. Heat Mass Transf. 33 (2) (2006) 142–150.
[7] L.H. Dai, Z.P. Huang, R. Wang, A generalized self-consistent mori–tanaka model for predicticting the effective moduli of coated inclusion based composites, Acta Mech. Solida Sin. 20 (3) (1999) 187–194.
[8] S. Mercier, A. Molinari, M.E. Mouden, Thermal conductivity of composite material with coated inclusions: Applications to tetragonal array of spheroids, J. Appl. Phys. 87 (7) (2000) 3511–3519.
[9] S. Lu, J. Song, Effective conductivity of composites with spherical inclusions: Effect of coating and detachment, J. Appl. Phys. 79 (2) (1996) 609–618.
[10] H.J. Böhm, S. Nogales, Mori–tanaka models for the thermal conductivity of composites with interfacial resistance and particle size distributions, Compos. Sci. Technol. 68 (5) (2008) 1181–1187.
[11] F.L. Chen, C.P. Jiang, A recurrence formula for the prediction of the effective thermal conductivity of fiber reinforced composites with an inhomogeneous interphase, Acta Meter. Compos. Sin. 26 (4) (2009) 151–155.
[12] H.S. Cawslow, J.C. Jeager, Conduction of Heat in Solids, Oxford Clarendon Press, Oxford, 1959.
[13] J. Chatterjee, D.P. Henry, F. Ma, P.K. Banerjee, An efficient BEM formulation for three- dimensional steady-state heat conduction analysis of composites, Int. J. Heat Mass Transf. 51 (5) (2008) 1439–1452.
[14] H. Hatta, M. Taya, Equivalent inclusion method for steady state heat conduction in composites, Internat. J. Engrg. Sci. 24 (7) (1986) 1159–1172.
[15] S.J. Park, T.H. Kwon, Sensitivity analysis formulation for three-dimensional conduction heat transfer with complex geometries using a boundary element method, Internat. J. Numer. Methods Engrg. 39 (16) (2015) 2837–2862.
[16] X. Qin, J.M. Zhang, L. Liu, G. Li, Steady-state heat conduction analysis of solids with small open-ended tubular holes by BEM, Int. J. Heat Mass Transf. 55 (23–24) (2012) 6846–6853.
[17] T.J.R. Hughes, The Finite Element Method - Linear Static and Dynamic Finite Element Analysis, Prentice-Hall, Englewood Cliffs, New Jersey, 1987.
[18] R.M. Christensen, Mechanics of Composite Materials, John Wiley & Sons, New York, 1979.
[19] C.Y. Dong, An interface integral formulation of heat energy calculation of steady state heat conduction in heterogeneous media, Int. J. Heat Mass Transf. 90 (10) (2015) 314–322.
[20] C.Y. Dong, Boundary integral equation formulations for steady state thermal conduction and their applications in heterogeneities, Eng. Anal. Bound. Elem. 54 (2015) 60–67.
[21] T.J.R. Hughes, J.A. Cottrell, Y. Bazilevs, Isogeometric analysis: CAD, finite elements, NURBS, exact geometry and mesh refinement, Comput. Methods Appl. Mech. Eng. 194 (39–41) (2005) 4135–4195.
[22] J.A. Cottrell, T.J.R. Hughes, Y. Bazilevs, Isogeometric Analysis: Toward Integration of CAD and FEA, John Wiley & Sons, Chichester, 2009.
[23] W.A. Wall, M.A. Frenzel, C. Cyron, Isogeometric structural shape optimization, Comput. Methods Appl. Mech. Engrg. 197 (33–40) (2008) 2976–2988.
[24] Y. Bai, C.Y. Dong, Z.Y. Liu, Effective elastic properties and stress states of doubly periodic array of inclusions with complex shapes by isogeometric boundary element method, Compos. Struct. 128 (2015) 54–69.
[25] A. Aimi, M. Diligenti, M.L. Sampoli, A. Sestini, Isogemetric analysis and symmetric Galerkin BEM, Appl. Math. Comput. 272 (2016) 173–186.
[26] G. Beer, I.M. Smith, C. Duenser, The Boundary Element Method with Programming for Engineers and Scientists, Springer Wien, New York, 2008.
[27] R.N. Simpson, S.P.A. Bordas, H. Lian, J. Trevelyan, An isogeometric boundary element method for elastostatic analysis: 2D implementation aspects, Comput. Struct. 118 (6) (2013) 2–12.
[28] C.Y. Dong, K.Y. Lee, A new integral equation formulation of two-dimensional inclusion-crack problems, Int. J. Solids Struct. 42 (18–19) (2005) 5010–5020.